ARCHIVIO ISTITUZIONALE
DELLA RICERCA

Alma Mater Studiorum Università di Bologna
Archivio istituzionale della ricerca

Experimental investigation on the effect of spot diameter on continuous-wave laser welding of copper and aluminum thin sheets for battery manufacturing

This is the final peer-reviewed author's accepted manuscript (postprint) of the following publication:

Published Version:
Dimatteo, V., Ascari, A., Liverani, E., Fortunato, A. (2022). Experimental investigation on the effect of spot diameter on continuous-wave laser welding of copper and aluminum thin sheets for battery manufacturing. OPTICS AND LASER TECHNOLOGY, 145(1), 1-12 [10.1016/j.optlastec.2021.107495].

Availability:
This version is available at: https://hdl.handle.net/11585/830766 since: 2024-05-27

Published:

DOI: http://doi.org/10.1016/j.optlastec.2021.107495

Terms of use:

Some rights reserved. The terms and conditions for the reuse of this version of the manuscript are specified in the publishing policy. For all terms of use and more information see the publisher's website.

This item was downloaded from IRIS Università di Bologna (https://cris.unibo.it/).
When citing, please refer to the published version.

(Article begins on next page)

27 July 2024

This is the final peer-reviewed accepted manuscript of:

[DiMatteo, V., Ascari, A., Liverani, E., Fortunato, A., Experimental investigation on the effect of spot diameter on continuous-wave laser welding of copper and aluminum thin sheets for battery manufacturing. Optics & Laser Technology 145, 107495 (2022)]

The final published version is available online at: **https://doi.org/10.1016/j.optlastec.2021.107495]**

Terms of use:

Some rights reserved. The terms and conditions for the reuse of this version of the manuscript are specified in the publishing policy. For all terms of use and more information see the publisher's website.

This item was downloaded from IRIS Università di Bologna (https://cris.unibo.it/)

When citing, please refer to the published version.

Experimental investigation on the effect of spot diameter on continuous-wave laser welding of copper and aluminum thin sheets for battery manufacturing

Dimatteo Vincenzo[1], Ascari Alessandro[1], Liverani Erica[1], Fortunato Alessandro[1]

[1]Department of Industrial Engineering, Alma Mater Studiorum – University of Bologna, Viale del Risorgimento 2, 40136, Bologna, Italy.
Corresponding author: Vincenzo Dimatteo
e-mail address: vincenzo.dimatteo4@unibo.it

Abstract

Welding of dissimilar materials, particularly copper and aluminum alloys, has gained considerable industrial interest in many different electric and electronic fields, such as the production of lithium-ion batteries for automotive applications. The differences in physical and chemical properties of these materials make fusion welding processes difficult to apply due to the formation of hard and brittle intermetallic compounds that impair both mechanical and electrical performance. In this paper, the effect of spot diameter on dissimilar laser autogenous lap-welding of copper and aluminum was studied. Experiments were conducted using a mid-power fiber laser source equipped with a galvo scanner and two different focal lengths to obtain two different spot diameters. The results showed that a smaller spot diameter promoted the formation of sound weld beads with better control of penetration depth, reduced mixing of the base metals and lower laser power requirements. By selecting the correct process parameters, good mechanical properties and low contact resistance could be obtained with both focal lengths. SEM-EDX analysis confirmed that a smaller spot diameter minimized the formation of copper rich phases in the weld bead.

Keywords: Dissimilar laser welding, Battery manufacturing, Copper and aluminum thin sheets, High reflectivity materials

1. Introduction

Joining processes for aluminum and copper in a dissimilar configuration have received much attention over recent years due to the unique properties of these materials such as high electrical conductivity, low weight and good corrosion resistance. An important field of application, amongst electric and electronic devices, lies within the automotive industry in the area of e-mobility.

Electro mobility will become increasingly important over coming years as many governments start to ban combustion engines to decrease the environmental impact of transportation, for example by

prohibiting their sale and their circulation within city centers. As a result, there will be a gradual shift from fossil fuel cars to electric vehicles (EVs) and hybrid-electric vehicles; thus, modern electric cars will gain popularity because of market factors and technological developments in e-mobility **[1]**. The heart of an EV lies within the battery pack, which consists of a large number of interconnected cells. Lithium-Ion (Li-ion) rechargeable batteries are the most commonly used technology **[2]**. There are three different types of cells used for vehicle propulsion, including cylindrical, prismatic and pouch cells. Li-ion pouch cells are widely used in high-performance vehicles thanks to their high energy density. The current collectors of pouch cells are manufactured using thin pure aluminum (cathode) and copper (anode) sheets.

Within this field, much work has been devoted to studying dissimilar welding of copper and aluminum thin sheets to generate proper electrical connections for producing batteries and related components **[3]**. Further to the high optical reflectivity of both copper and aluminum at the wavelength of common high-power industrial lasers, dissimilar laser welding of aluminum and copper must deal with many other difficulties, including different physical properties of the two parent metals, the formation of intermetallic compounds and requirements for thorough control of penetration depth and a clean and spatter-free process **[4]**. Many authors have studied conventional joining process such as ultrasonic welding and friction stir welding **[5-6]**. Although it is possible to generate weld seams with good properties, conventional technologies are characterized by low flexibility and repeatability. Within this context, many studies have been conducted in the field of autogenous welding by laser radiation, exploiting the unique properties of laser beams such as mono-chromaticity and spatial and temporal coherence. **[7-8]**.

Despite being widely used in many different applications within the electronic and electrical industry, joining of aluminum and copper presents several challenges due to differences in the physical and chemical properties of the two materials **[9]**. By analyzing the Al-Cu binary system, it can be observed that different intermetallic compounds (IMC) can form, which are characterized by brittleness, high hardness and high electrical resistivity **[10]**; the properties of various IMC are reported in table 1. In order to obtain a reliable weld seam, the formation of hard and brittle IMC must be avoided or minimized. In line with these considerations, many authors have stressed the role of equipment and process parameters on the possibility of producing sound copper-aluminum joints with industrially reliable laser processes. Fetzer et al**.[8]** explored the possibility of exploiting laser beam oscillation to control the depth and width of the weld bead during lap-welding of 1 mm thick aluminum onto 1 mm thick copper sheets. The authors found that both element mixing in the fused zone and crack formation were reduced for larger oscillation amplitudes; however, despite the results on how the oscillation parameters affect the mixing of the metal are satisfactory there are no data on how the

latter can affect the electrical and mechanical properties of the joint. Schmalen et al. **[11]** investigated the possibility of exploiting a modulated high brilliance laser source and beam oscillation to join 0.2 mm thick aluminum onto 0.5 mm thick copper sheets. They highlighted the fact that material mixing must be minimized in order to enhance the mechanical properties of the weld seam; anyway, the welding equipment provided for the use of a pulsed laser source which does not allow to obtain high process speeds. Ascari et al. **[12]** compared three different pulsed laser sources for lap-welding of 0.4 mm thick aluminum onto 0.3 mm thick copper sheets, demonstrating the important role played by the spot size during welding due to the high reflectivity and thermal conductivity of the base materials; in the presented paper the authors exploited the configuration with aluminum as upper material and furthermore the welding speeds are very low if compared to a continuous laser source. Schmalen et al.**[10]** studied the distribution of intermetallics during lap welding of aluminum and copper, finding that the thickness of intermetallic compounds must be maintained below a critical value to avoid reducing the properties of the joint. Lerra et al. **[7]** investigated the role of pulse distribution during welding of aluminum and copper sheets using a low brilliance laser, showing how good mechanical properties can be achieved by modulating the pulse shape; despite good results in terms of mechanical and electrical properties have been obtained by the authors, no investigations on copper to aluminum configuration has been carried out probably due to the low brilliance of the laser source exploited. Dimatteo et al. **[13]** and Fortunato et al. **[14]** investigated the application of a single-mode laser source for remote welding of Al-Cu and Cu-Al in an overlap configuration, demonstrating the feasibility of laser welding to obtain weld seams with good mechanical properties; the authors showed that the exploitation of a single high-brightness laser source allowed to investigate all the configurations described and allowed to keep the heat input in the weld bead very low. Reisgen et al. [15] studied the influence of the degree of dilution on the electrical properties of the laser beam welded aluminum and copper in butt joint configuration under reduced ambient pressure; however, despite good results in terms of joint's performance have been obtained, laser beam weld under vacuum is difficult to apply in the industrial field. Jarwitz et al. [16] investigated the laser welding of aluminum to copper with a thickness of 1 mm by means of a spatial oscillation of the laser beam and found that high width/depth ratios of the weld seam could improve the electrical properties of the connections although the process has proved feasible, the thicknesses investigated are much greater than those used in real applications. The influence of laser power on microstructure and mechanical properties of aluminum (6061), not properly used for electrical applications due to the presence of alloying elements, and 110 copper joints in dissimilar configurations has been studied also by Yan et al [17]; they founded that with an increase of laser power, more copper diffuses into the weld seam which results in the formation of harder and brittle intermetallic compounds. The above-mentioned literature

clearly underlines growing interest towards this specific topic; however, welding configurations comprising copper as the upper material have seen little attention, while the effect of different focal spot sizes on the resulting mechanical and electrical properties has not yet been fully addressed.

The aim of the present work was therefore to analyze the influence of focal spot diameter on weld quality for joining of copper and aluminum in a lap joint configuration. In order to make the investigation more effective, two different focal lengths were exploited: 163 mm for standard high-power density applications and 420 mm for remote welding. After defining a feasibility window, the effects of power and welding speed on the weld bead geometry were assessed. SEM-EDX analysis allowed considerations to be made in relation to the composition of IMC formed after welding. Subsequently, samples were mechanically analyzed with tensile and electrical contact resistance tests.

Table 1: Characteristic of intermetallic compounds **[9-11]** .

Phase	**Nominal composition**	**Chemical composition [% at. Cu]**	**Spec. Electrical resistance [μΩ cm] [18]**	**Hardness [HV]**
(Al)		0-2.2	2.4	36
Θ	Al_2Cu	31.9-33	8.0	630
η	AlCu	51.9-54.8	11.4	905
ζ	Al_3Cu_4	56-57.5	12.2	930
γ	Al_4Cu_9	64-69	14.2	770
(Cu)		80.3-100	2.0	75

2. Experimental procedure

Pure copper (Cu > 99.5 %, 0.3 mm thick) coated with a thin (2.5 µm) electroplated nickel layer and commercially pure aluminum (EN-EW 1050, 0.45 mm thick) sheets were used for experiments. Test specimens comprised a 60x45 mm Cu sheet welded onto a 60x45 mm Al sheet in a lap-joint configuration with the copper sheet on top (see fig. 1(c)). The overlap between the two sheets was 10 mm, while the length of the weld bead was kept shorter than the width of the specimen to avoid extending the fusion zone to the edges of the sheets and forming fusion notches.

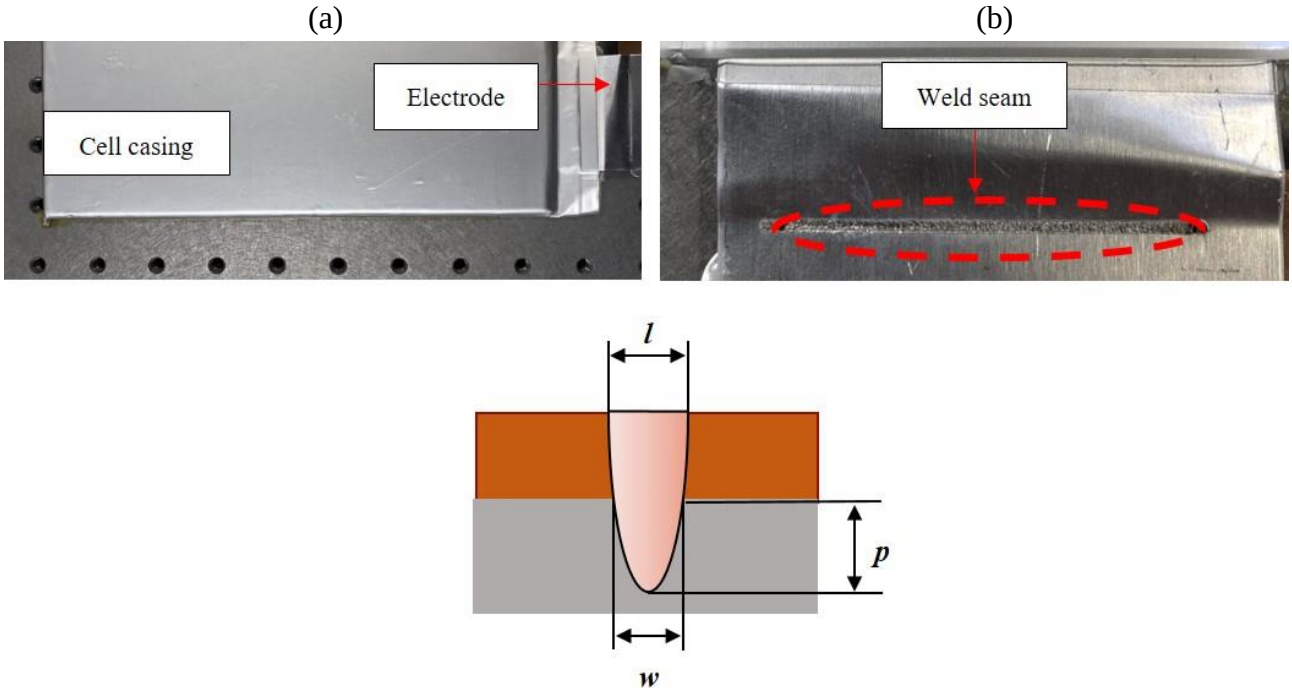

Fig.1: Example pouch cell structure (a), type of joint used (b) and weld seam characteristics (c).

A clamping device was designed to guarantee correct adhesion between the sheets during the joining process. Samples were cleaned with acetone before welding. An nLight Alta 3.0 kW continuous-wave Yb:Fiber laser (BPP < 2.8 mm*mrad) with a wavelength of 1070 nm was used for all trials. The feeding fiber core diameter was 50 µm while the focusing optics comprised a Scanlab HurryScan 30 galvo scanner combined with two Wavelength fused silica high power F-Theta lenses with focal lengths of 163 mm and 420 mm, respectively. The focusing optics were mounted on a 6-axis anthropomorphic robot (Yaskawa-Motoman HP-20) that allowed movement of the optics within the welding area. During the welding process, the head was kept stationary while movement of the beam was performed by the galvos. No shielding gas was used; however, a high-pressure lateral air jet was used to protect the scanning optics. In order to achieve a comparison, the galvo scan head was equipped with two different F-Theta lenses that allowed generation of two different spot dimensions.

The laser beam was focused on the surface of the top sheet without tilting the head. Optics specifications are shown in table 2.

Table 2. Optics specifications.

	Lens 1	**Lens 2**
Collimation length [mm]	120	120
Focal length [mm]	163	420
Magnification rate	1.36	3.5
Spot diameter [µm]	68	175
Rayleigh length [mm]	0.6	3.8

Linear welds were performed with both lenses by varying the laser power and feed rate in order to define a process window and evaluate how the process parameters affected weld bead formation. Laser power was between 600 W and 1000 W for the smaller spot size and between 1000 W and 1500 W for the larger one. The welding feed rate was varied from 150 mm/s to 250 mm/s for both configurations. With the aim of comparing the two spot diameters, parameters were chosen to obtain roughly the same range of energy density (power density·interaction time) for both focal lengths (see tables 3 and 4).

Table 3. Experimental parameters - 160 mm lens (Spot diameter 68 µm).

Sample	**Power [W]**	**Welding speed [mm/s]**	**Power Density [MW/cm^2]**	**Energy Density [MJ/mm^2]**
A1	600	150	18.08	0.7835
A2	600	200	18.08	0.5576
A3	600	250	18.08	0.4701
B1	800	150	24.11	1.0447
B2	800	200	24.11	0.7835
B3	800	250	24.11	0.6268
C1	1000	150	30.14	1.3059
C2	1000	200	30.14	0.9794
C3	1000	250	30.14	0.7835

Table 4. Experimental parameters - 420 mm lens (Spot diameter 175 µm).

Sample	Power [W]	Welding speed [mm/s]	Power Density [MW/cm^2]	Energy Density [MJ/mm^2]
D1	1000	150	4.16	0.4850
D2	1000	200	4.16	0.3638
D3	1000	250	4.16	0.2910
E1	1250	150	5.20	0.6063
E2	1250	200	5.20	0.4547
E3	1250	250	5.20	0.3638
F1	1500	150	6.24	0.7276
F2	1500	200	6.24	0.5457
F3	1500	250	6.24	0.4365

Preliminary observations of the weld seam were performed with a stereomicroscope to obtain information regarding spatters and the possible presence of other defects such as micro-cracks. In order to characterize the weld beads in terms of dimensions and morphology, cross sections were prepared by mounting the samples in resin and polishing them with SiC paper followed by alumina in suspension. No etchant was used to identify the weld seam geometry. The specimens were also mechanically characterized via shear tensile tests performed at a crosshead speed of 0.025 mm/s with an Instron 8033 testing machine equipped with a 10 kN load cell. It must be noted that the samples used for tensile tests did not comply with any specific standard in relation to their shape and dimensions, as the aim was to qualitatively evaluate the overall strength of the joint. For each combination of parameters, three specimens were welded, and the average value of maximum failure load calculated. Electrical resistance was measured at room temperature via the four-point method with a test length of 20 mm; the set-up used has been reported in figure 2. Measurements were performed with a Chauvin Arnaux CA 6255 micro-ohmmeter characterized by an accuracy of 0.1 μΩ and a measurement current of 10 A for 20 s. A scanning electron microscope (SEM) equipped with an energy dispersive X-ray spectrometer (EDS) was used to analyze the weld specimens with the aim of obtaining information about the chemical composition of the formed IMC.

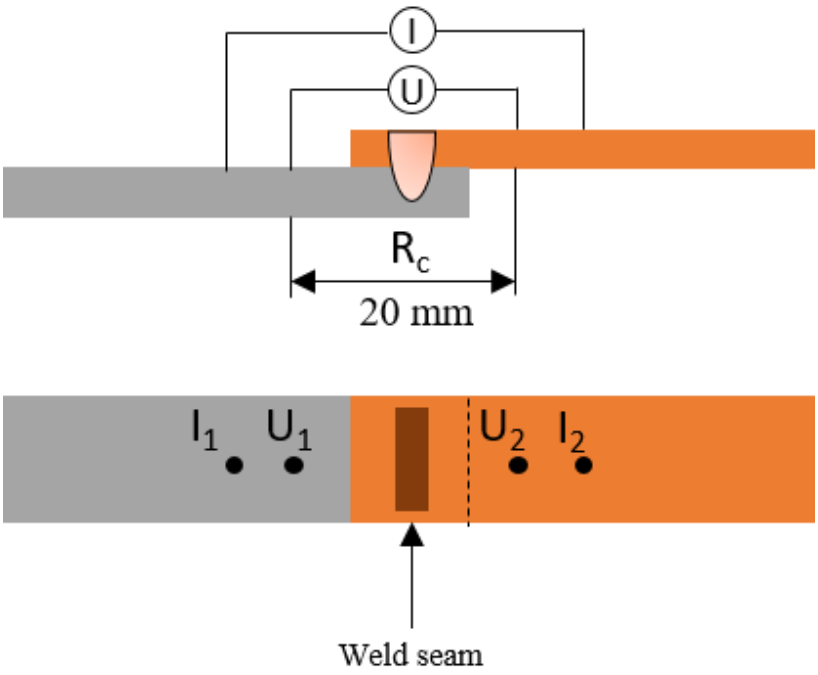

Fig.2: Electrical contact resistance set-up.

3. Results

3.1. Optical microscopy

Microscope and stereomicroscope images of welded specimens obtained with the smaller spot size are shown in figure 3. The set of parameters that were chosen allowed weld seams without defects (micro-cracks) to be obtained, as can be seen from the cross sections. The weld beads were fairly regular along the entire surface, with negligible presence of spatters. With this configuration, good welding in terms of weld seam morphology was obtained with a wide range of process parameters (see fig.7). The interface width was not clearly influenced by the energy density, with values varying between 150 and 250 µm. As energy density increased, penetration depth into the lower aluminum sheet increased, reaching full penetration with the highest values of this parameter. Full penetration involved evident mixing of the two materials within the interface area.

(a)
Power = 600 W, Welding speed = 200 mm/s

(b)
Power = 600 W, Welding speed = 150 mm/s

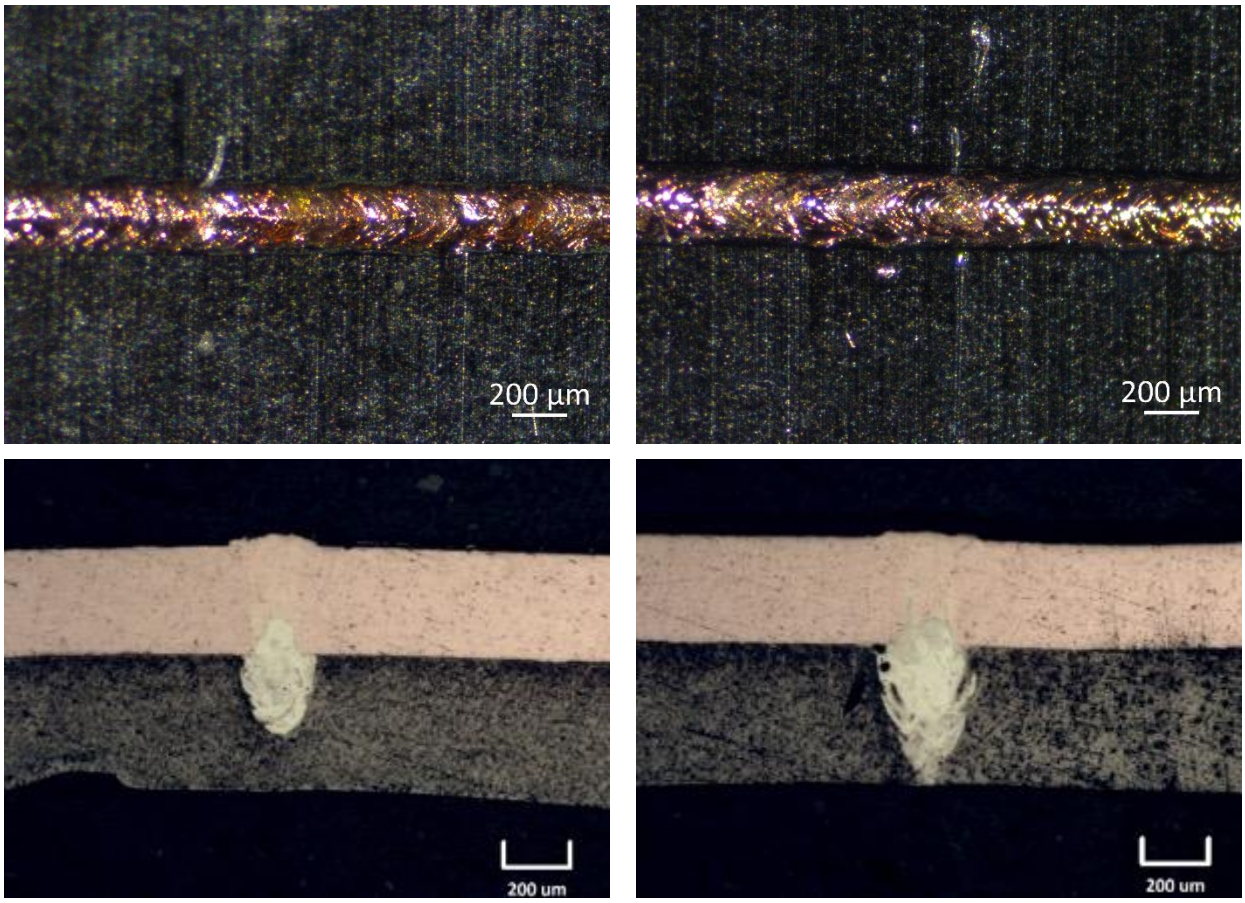

Fig.3. Top and cross-section of specimen welded with spot diameter of 65 µm.

With the larger spot size, higher power was required to overcome the high reflectivity of the upper copper layer. Microscope and stereomicroscope images of weld seams obtained in this configuration are shown in figure 4. In this case, transversal and longitudinal cracks were found in some of the weld seams. This effect was due to the higher specific heat input in this configuration, which caused the formation of a larger amount of intermetallics (IMC) and promoted a thermal cycle that made the bead prone to cracking. Crack formation may be caused by residual stresses or differences in the thermal expansion coefficient and hardness of Al-Cu IMC. When the heat input is too high, temperature increases are larger, thus producing higher residual stresses with the appearance of cracks along the weld seam.

(a)
Power = 1500 W, Welding speed = 200 mm/s

(b)
Power = 1500 W, Welding speed = 150 mm/s

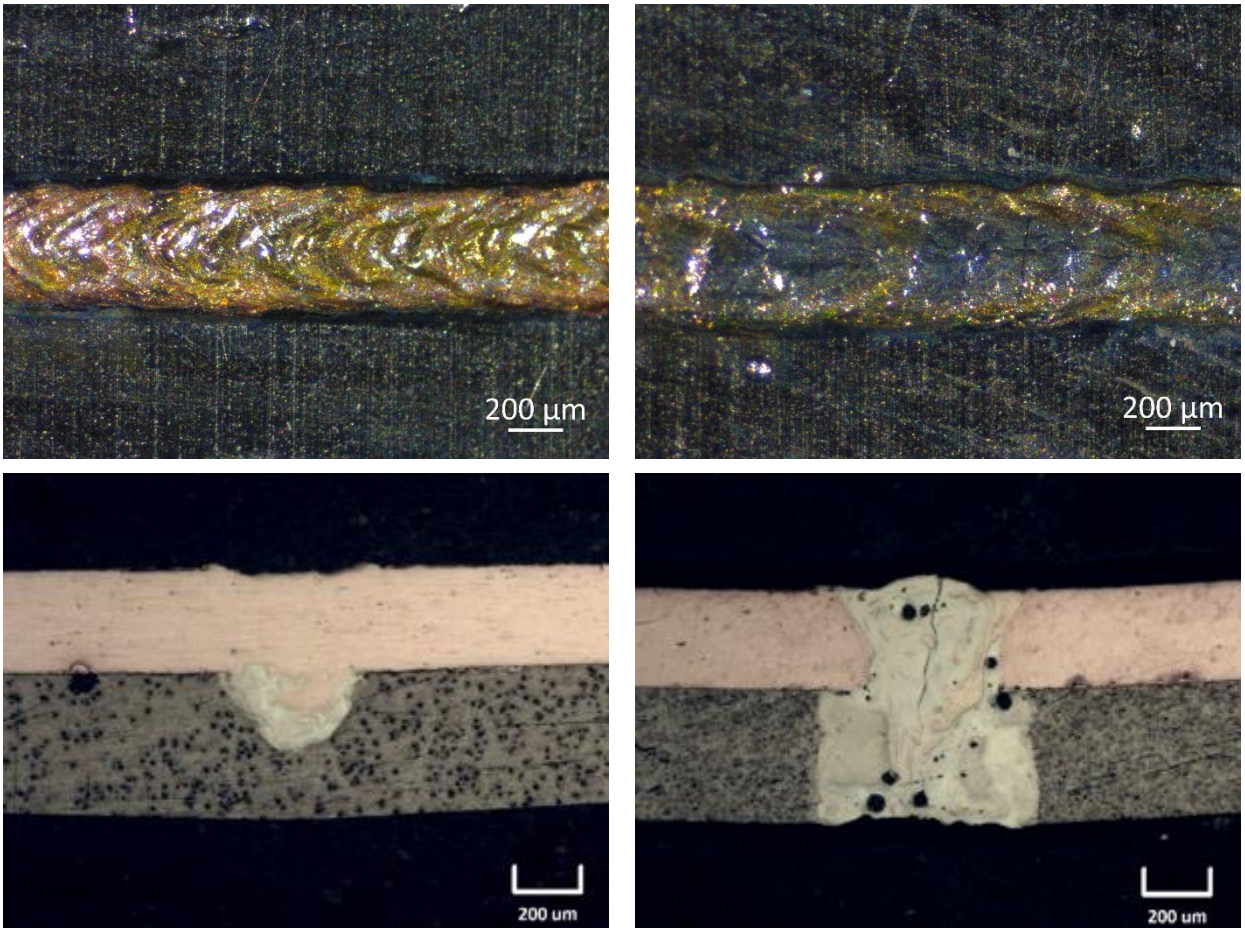

Fig.4. Top and cross-section of specimen welded with spot diameter of 175 µm.

Once weld seam cross-sections were obtained, it was possible to measure their geometry. Weld width was measured at the interface between the two sheets, while the penetration depth into the lower sheet was measured from the interface between the two materials. The correlation between laser power, welding speed and interface width is reported in fig.5(a) for a spot diameter of 68 µm. At 150 mm/s, weld width increased from 127 µm at 600 W to 220 µm at 800 W, after which no further differences in weld width were recorded with increasing laser power. In Figure 5(b) penetration depth is reported as a function of laser power. At 150 mm/s, full penetration was obtained at all power levels employed during the activity. At 250 mm/s, the penetration depth increased with laser power from 150 µm at 600 W to 390 µm at 1000 W.

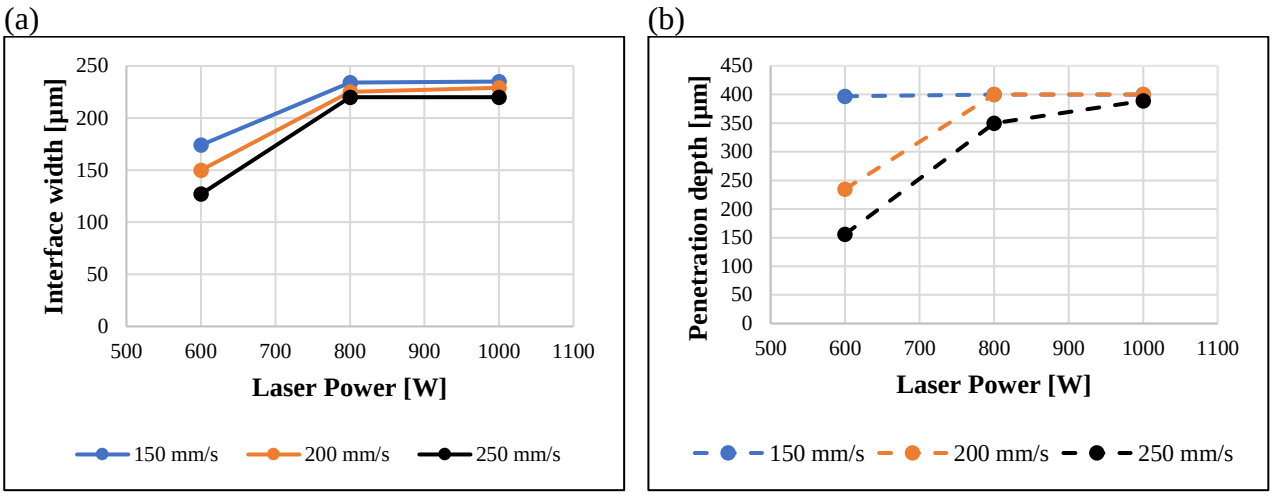

Fig.5: Interface width (a) and penetration depth (b) as a function of laser power obtained with spot diameter of 68 µm.

Using the 420 mm focal length (see figure 7), no welding was achieved at 250 mm/s regardless of the laser power. The interface width at 150 and 200 mm/s instead increased with laser power. By observing figure 6(b), it can be noted that partial penetration could only be obtained with a limited range of parameters. Values of 60 µm and 150 µm were obtained with a laser power of 1250 W and 1500 W at 200 mm/s.

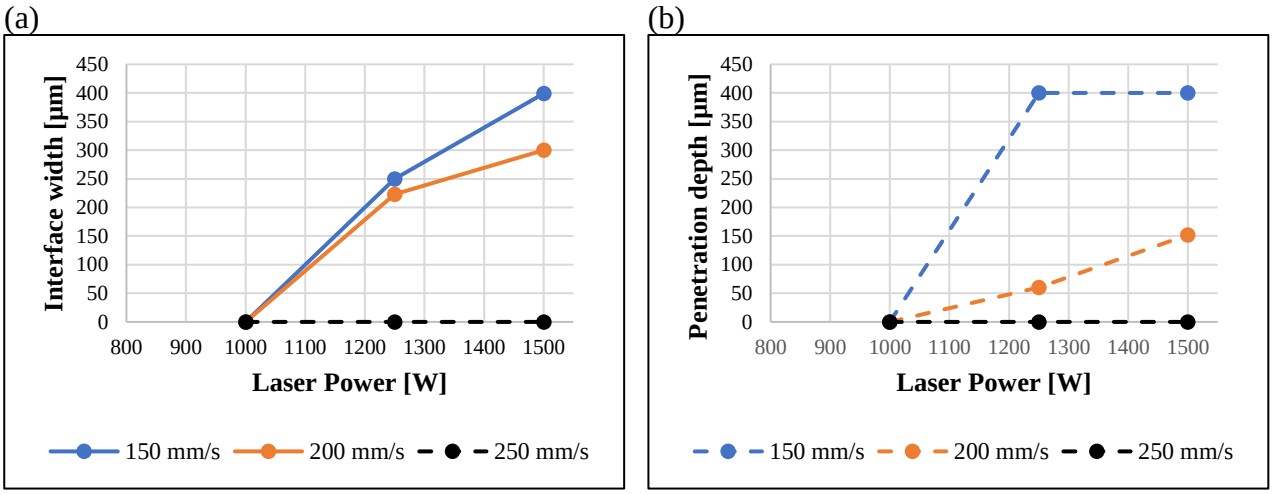

Fig.6: Interface width (a) and penetration depth (b) as a function of laser power obtained with spot diameter of 175 µm.

Cross-section images obtained with the optical microscope allowed a process feasibility window to be defined in terms of power and welding speed, as reported in fig. 7. With high energy input, a weld seam with full penetration was obtained, leading to high levels of mixing and a greater probability of brittle and hard intermetallic compounds being present (fig.7(c)). This joint shape also potentially

creates problems as it may damage nearby components during the assembly of a battery pack. On the other hand, a weld seam with partial penetration reduced such problems as mixing of the materials involved only a small portion of the bead without breaking through the lower sheet (fig.7(b)). Due to physical and optical properties of copper, the larger spot size required higher power to melt the material. In this case, adjustment of the power and speed was difficult because the weld seam shifted from a no-welding condition to full penetration with cracks and pores very quickly. Good results in terms of weld seam morphology were nonetheless obtained with a welding speed of 200 mm/s and power of 1250 and 1500 W. A spot diameter of 65 µm favored a wider process window with better control of the penetration depth and dilution of the base metals. Due to high power density, a no-welding condition was never obtained with the parameters used during these tests. With a welding speed of 250 mm/s and a power of 600 and 800 W, weld seams with partial penetration and reduced presence of defects were obtained. It can be concluded that a smaller spot allows welding with reduced overall power, thus reducing the total heat input during the process. Furthermore, higher welding speeds can be employed, enabling greater productivity from manufacturing point of view and less liquid interaction of welded metals.

(a)

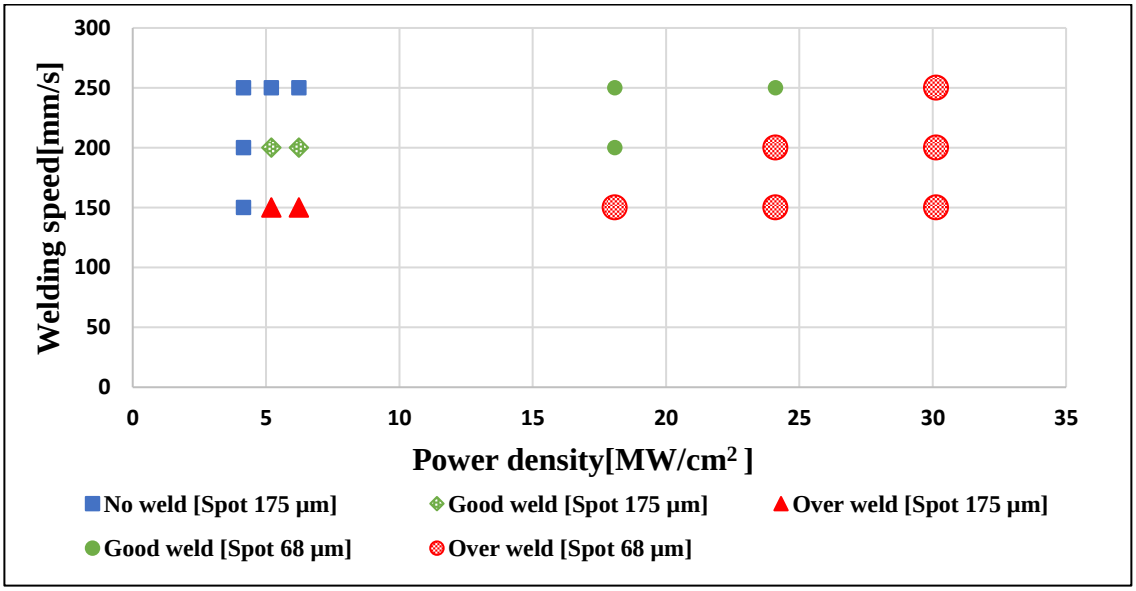

(b) (c)

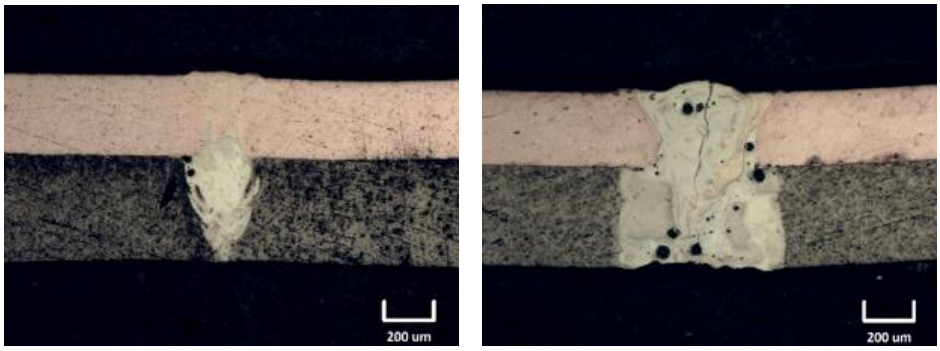

Fig.7: Feasibility process window (a), example of good weld condition (b) and over weld condition (c).

3.2. SEM-EDX analysis

SEM-EDX analysis was performed with the aim of obtaining information about the chemical composition of intermetallic compounds formed during welding and how the spot diameter affected their formation. For this purpose, two samples obtained with different levels of energy input were analyzed for each spot size, considering different zones of the weld seam. Cross-section images of sample A2 are shown in fig.8. When partial penetration took place, mixing between the two metals was limited to the aluminum sheet and a small part of the copper sheet. The chemical composition of the marked points in fig. 8 are listed in table 5. In the upper part of the weld seam (fig.8 (A)), presence of the $\Theta(Al_2Cu)$ phase was detected in the form of serrated dendrites. At the interface zone and in the lower part of the weld seam, the copper content never exceeded 25 at%, resulting in the detection of Al-Cu eutectic alloy with a vermicular shape. Due to the low heat input and reduced cooling time, the melt pool and thus the base metals were not subjected to violent fluctuations in copper content, resulting in a homogenous phase composition **[19]**.

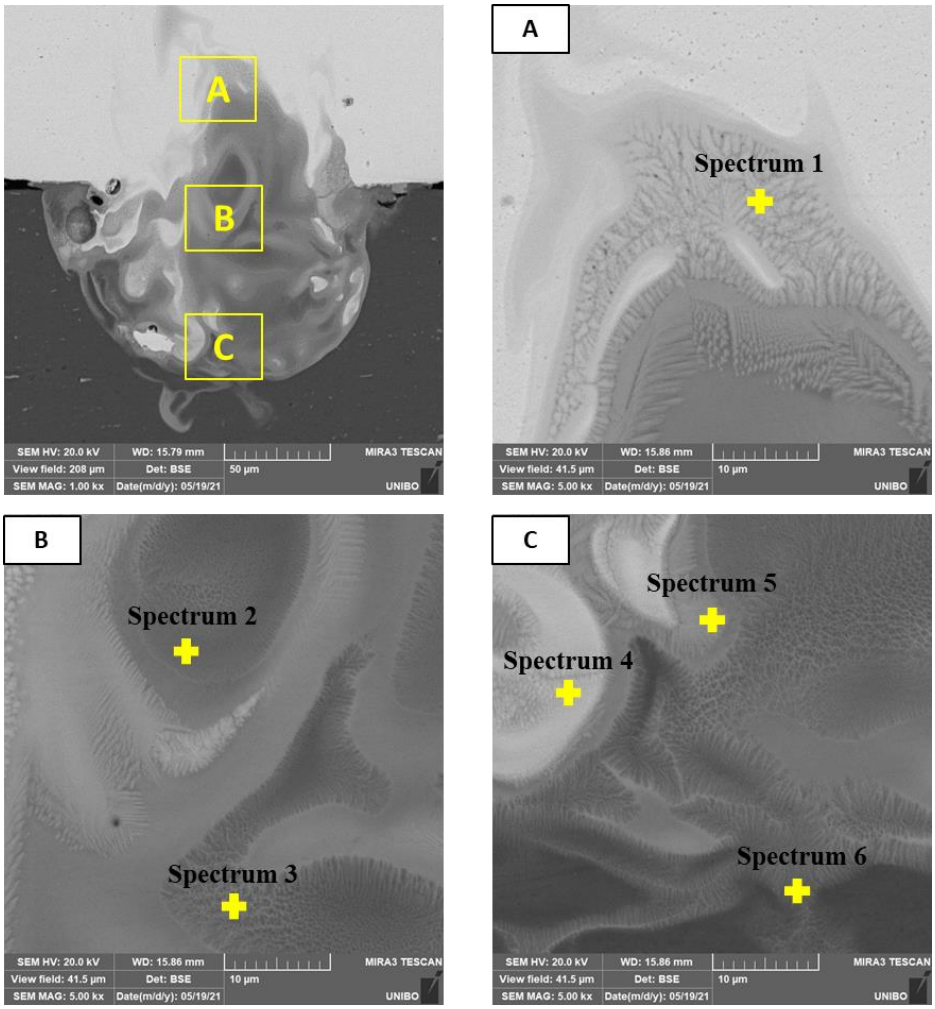

Fig. 8: SEM images of sample A2; Power = 600 W, Welding Speed = 200 mm/s, Spot diameter = 68 µm

Table 5: Chemical composition of denoted zones in fig.7

Spectrum	Al (at%)	Cu (at%)	O (at%)	Possible Phase
1	55.78	43.92	0.3	Θ(Al_2Cu)
2	82.05	15.02	2.85	Al-Cu eutectic
3	81.73	16.69	1.58	Al-Cu eutectic
4	44.43	54.98	0.59	η (AlCu)
5	71.17	27.75	1.08	Al+ Θ(Al_2Cu)
6	88.57	8.56	2.86	Al-Cu eutectic

Fig. 9 depicts cross-section images of sample C3. The chemical compositions of marked points are listed in table 6. By increasing the energy density from 0.5576 to 0.7835 MJ/mm^2, mixing was more pronounced and a greater quantity of copper was found in the upper part of the weld bead while molten aluminum flowed upward. As a result, the η (AlCu) and γ(Al_4Cu_9) phases were detected in the form of columnar grains. At the interface, in the transition zone (fig.9 (B)), the η (AlCu) phase was detected, while in the lower part of the weld seam, the Θ(Al_2Cu) phase and Al-Cu eutectic alloy

formed, as seen in the previous case (figure 8(C)). Since heating was concentrated in a small area and the interaction time was very low with the smaller spot diameter, the $\Theta(Al_2Cu)$ and $\gamma(Al_4Cu_9)$ phases formed in the weld seam due to their low formation energies**[20]**. The intermetallic compound layers formed as a result of chemical reactions via inter-diffusion of Al and Cu atoms between the copper and aluminum metals at the interface. As suggested in previous works, no spalling occurred through the formation of a stable intermetallic compound between the Al and Cu layers **[21]**.

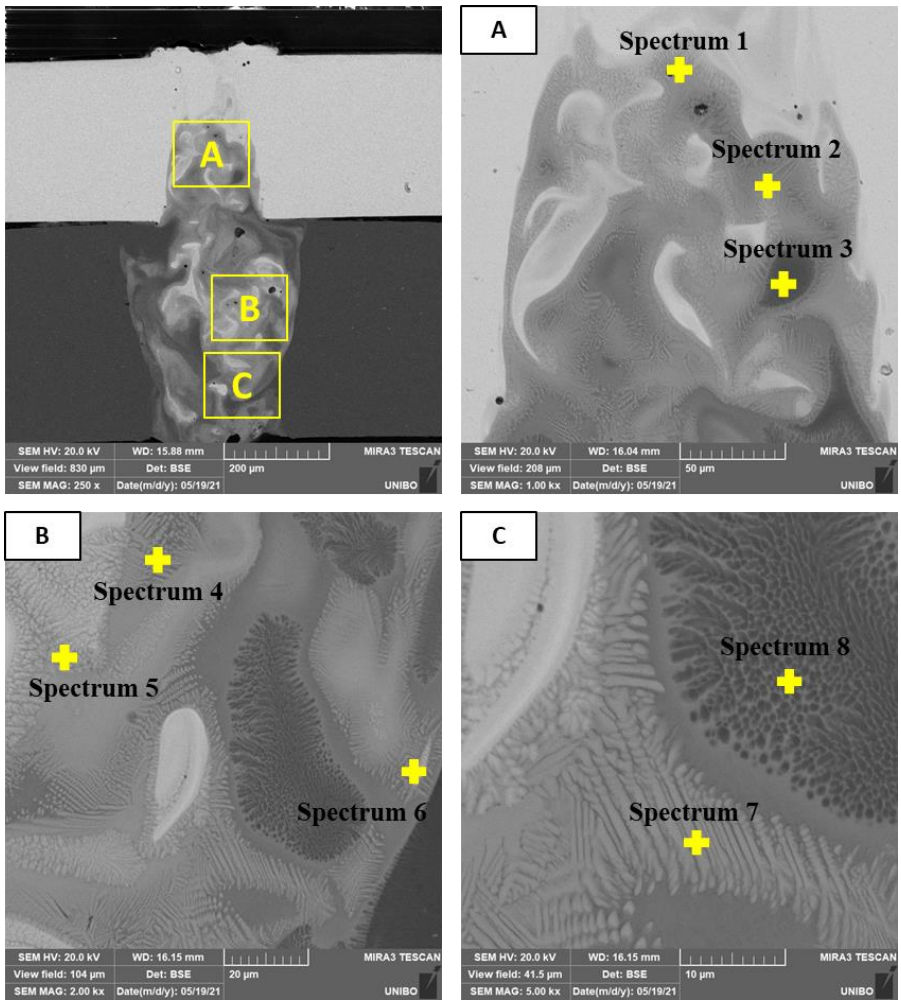

Fig. 9: SEM images of sample C3; Power = 1000 W, Welding Speed = 250 mm/s, Spot diameter = 68 µm

Table 6: Chemical composition of denoted zones in fig.9.

Spectrum	Al (at%)	Cu (at%)	O(at%)	Possible Phase
1	48.56	50.93	0.51	η (AlCu)
2	70.04	28.62	1.34	Al+ Θ(Al_2Cu)
3	93.26	2.58	4.15	Al-Cu eutectic
4	76.21	22.97	0.82	Al+ Θ(Al_2Cu)
5	64.66	34.75	0.59	Θ(Al_2Cu)
6	57.16	42.45	0.39	η (AlCu)
7	68.28	31.33	0.39	Θ(Al_2Cu)
8	90.97	6.31	2.72	Al-Cu eutectic

Cross-section SEM images of sample F2 obtained with the larger spot diameter, a laser power of 1500 W and a welding speed of 250 mm/s are shown in fig.10. By analyzing the image, it is possible to state that welding occurred via a conduction mode since mixing was limited in the lower part of the weld seam. The upper part of the joint consisted of copper in solid solution, while at the interface zone Θ(Al_2Cu) and η (AlCu) phases formed, characterized by columnar morphology. A composition change was also observed in zone C. Approaching the copper sheet, the Al-Cu eutectic was firstly detected followed by the Θ(Al_2Cu) phase as the amount of copper increased.

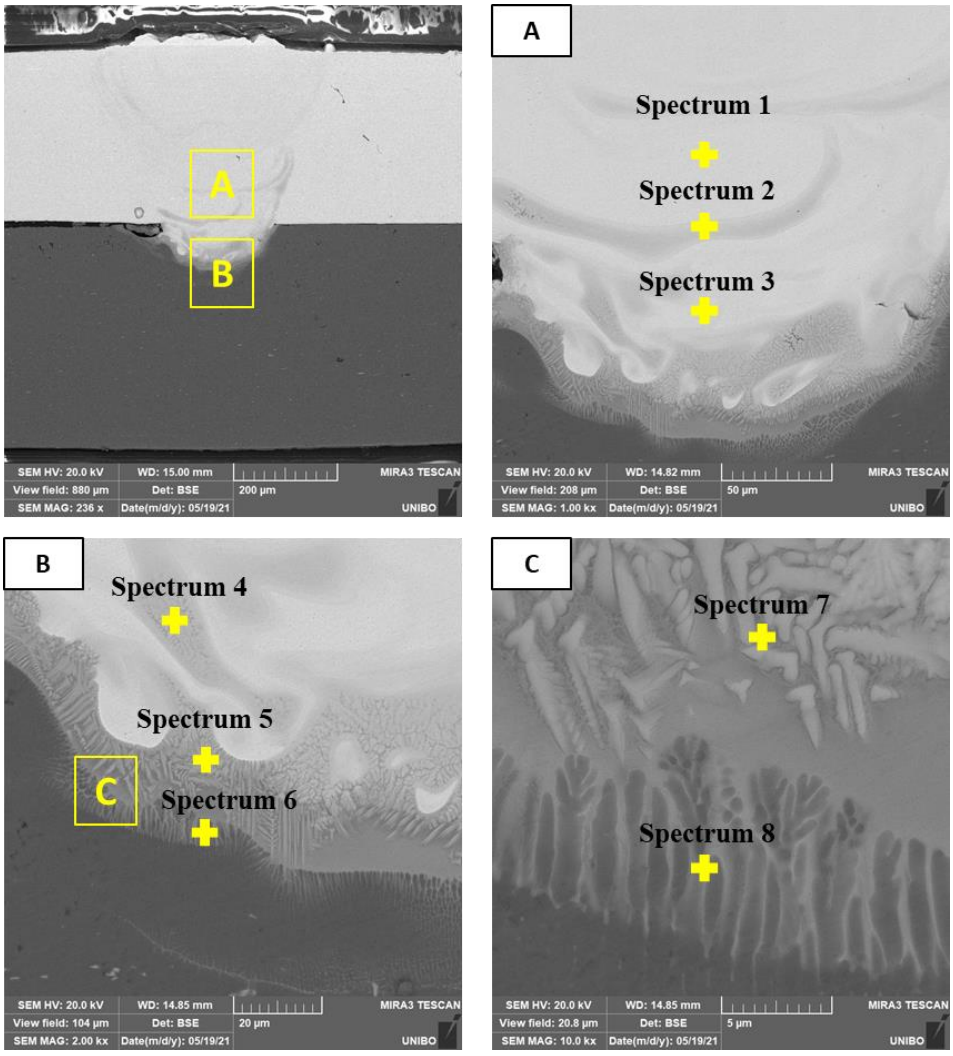

Fig. 10: SEM images of sample F2; Power = 1500 W, Welding Speed = 200 mm/s, Spot diameter = 175 µm

Table 7: Chemical composition of denoted zones in fig.11.

Spectrum	Al (at%)	Cu (at%)	O(at%)	Possible Phase
1	1.43	98.48	0.09	Cu
2	28.32	70.22	1.47	$\gamma(Al_4Cu_9)$
3	7.71	91.99	0.3	Cu
4	44.83	53.81	1.36	η (AlCu)
5	76.51	20.07	3.41	Al+ $\Theta(Al_2Cu)$
6	88.07	9.37	2.56	Al-Cu eutectic
7	68.28	31.33	0.39	$\Theta(Al_2Cu)$
8	90.97	6.31	2.72	Al-Cu eutectic

With the larger spot diameter, a small variation in welding speed at constant power led to elevated mixing of the base metals. When full penetration occurred, as shown in fig.11, large amounts of copper (more than 50 at%) were found throughout the weld bead. As a result, considering the Al-Cu binary system, the ζ(Al_3Cu_4) and γ(Al_4Cu_9) phases formed, which are the hardest and most brittle intermetallic compounds. Unlike the other phases, which are easily recognizable from their morphology, copper rich IMC are difficult to detect as they appear as a cluster of copper without a specific form. It is interesting to observe that most of the cracks propagated along the copper rich intermetallic compounds.

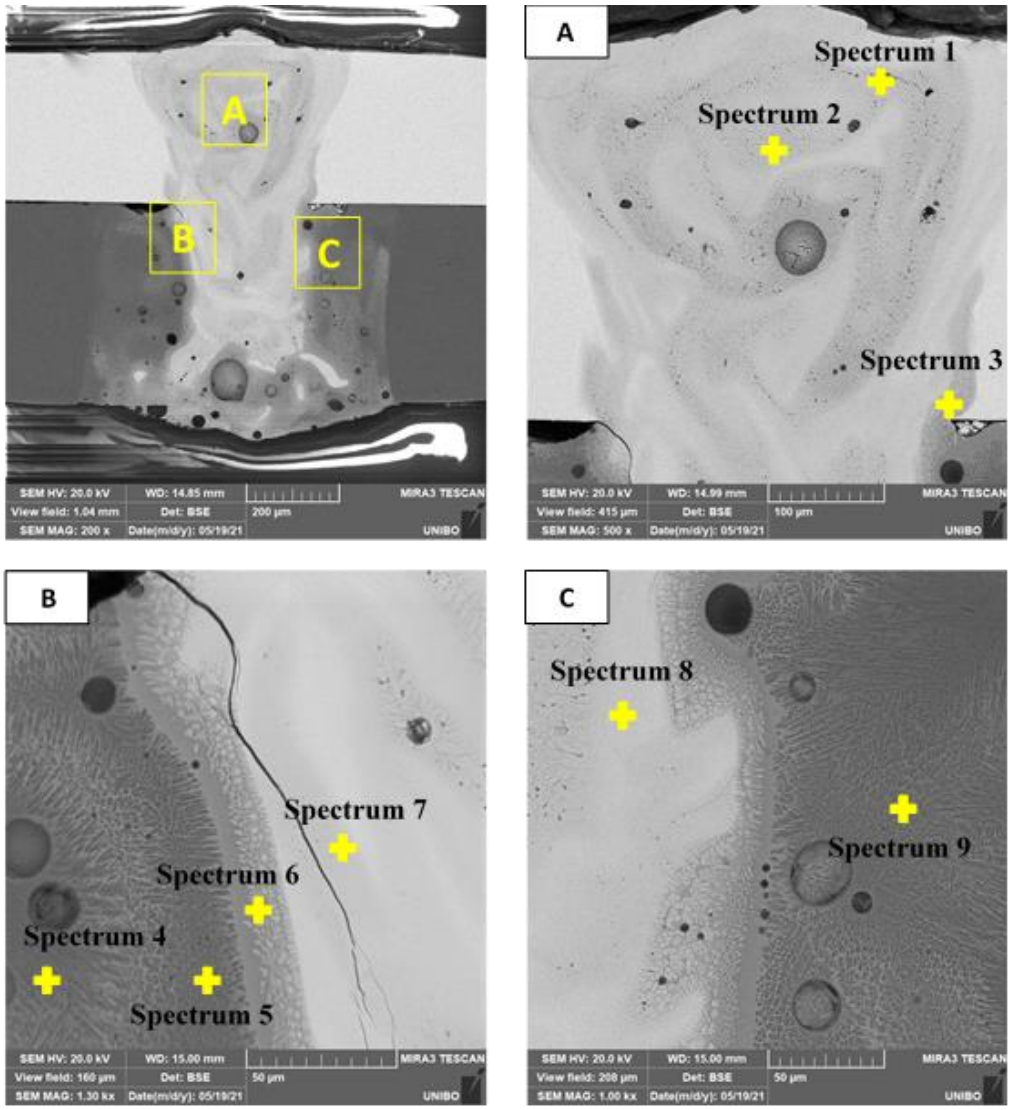

Fig. 11: SEM images of sample F2; Power = 1500 W, Welding Speed = 150 mm/s, Spot diameter = 175 µm

Table 8: Chemical composition of denoted zones in fig.13.

Spectrum	Al (at%)	Cu (at%)	O(at%)	Possible Phase
1	52.05	47.25	0.71	η (AlCu)
2	47.63	51.08	1.30	η (AlCu)
3	56.74	41.47	1.8	Θ(Al_2Cu)
4	91.46	4.29	4.25	Al-Cu eutectic
5	91.52	3.68	4.8	Al-Cu eutectic
6	68.06	31.47	0.48	Θ(Al_2Cu)
7	37.03	62.8	0.18	ζ(Al_3Cu_4)
8	46.04	53.79	0.17	η (AlCu)
9	93.28	4.03	2.69	Al-Cu eutectic

3.3. Mechanical results

Tensile shear tests were performed with the aim of obtaining information about the maximum load, fracture mode and failure position. Three different energy densities were chosen for each focal length to provide a comparison. Figure 12 reports the maximum load of the joints as a function of energy density. Tensile strength values between 750 N and 900 N were obtained with the larger spot, while values between 650 and 750 N were obtained with the smaller one. The relationship between energy density and maximum load was linear and decreasing in both analyzed configurations. For a given value of energy density, highest loads were obtained with the large spot due to the larger interface area characteristic of this configuration (see figures 5(a) and 6(a)).

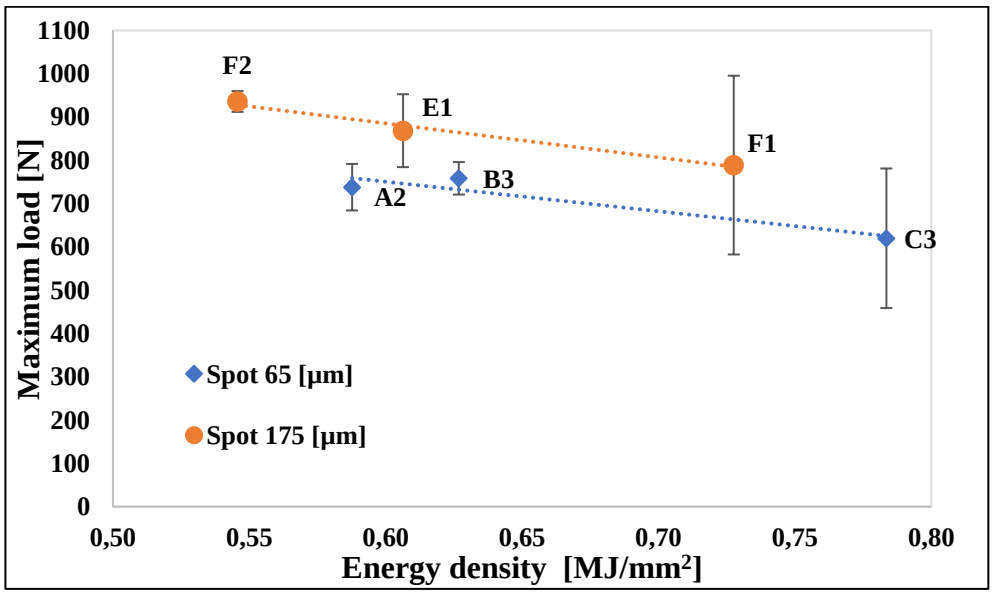

Fig.12: Shear tensile test results.

It is interesting to observe the role of spot size on the tensile test curves reported in figure 13. With reference to the red curve, plastic deformation was more limited and brittle fracture took place with the larger laser spot size. On the other hand, the plasticity of the joint was greater and ductile fracture took place with the smaller laser spot size.

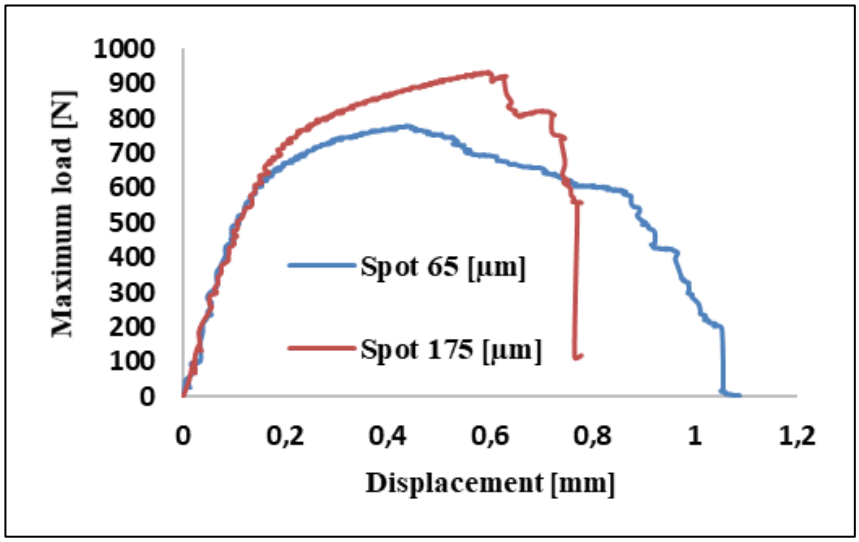

Fig.13: Example of tensile test curves.

Finally, fracture mechanisms were analyzed based on the corresponding microscope images shown in figure 14. It was found that fracture occurred in the fused zone on the copper side when welding was performed with a larger spot. Due to the increased spot area, higher powers were required to achieve fusion and welding of the sheets, thus leading to the formation of brittle and hard intermetallic compounds along the whole weld seam. Failure instead occurred at the interface between the two sheets when welding was performed with a smaller laser spot. Microscope images show that in this case mixing between the two materials, and thus the formation of intermetallic compounds, was reduced and limited to the interface. Higher mechanical strength and brittle fracture behavior with the larger spot size was therefore due to the formation of copper rich phases with higher hardness.

(a) (b)

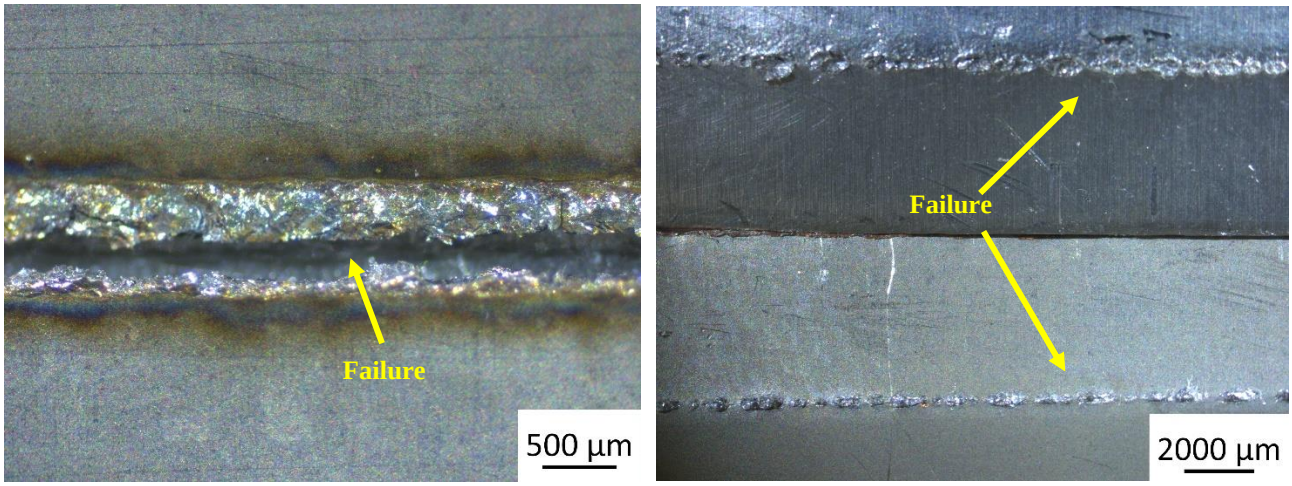

Figure 14: Schematic representation of failure mode: failure at fusion zone (a), failure at the interface (b)

3.4.Electrical contact resistance

Figure 15 reports the results of electrical contact resistance measurements. With the smaller spot diameter, values between 45 and 42 μΩ were recorded. Samples C3 and A2 exhibited highest values, which was likely due to the morphology of the weld bead. Higher energy density (sample C3) promoted both greater mixing of the base material and full penetration of the upper sheet into the lower one, resulting in the formation of hard and brittle intermetallic compounds with higher electrical resistivity. Sample A2 was instead characterized by a thin resistant section that also resulted in high contact resistance. A partial penetration condition (sample B3) allowed maximization of both electrical contact resistance and mechanical properties. With the larger spot diameter, values between 47 and 40 μΩ were measured. As noted before, higher contact resistance was obtained when full penetration, greater mixing and defect formation (pores and cracks) took place (samples F1 and E1). The correct choice of energy density allowed partial penetration to be obtained, optimizing the overall performance of the connections. It is important to note that electrical and mechanical properties are closely related as there is a linearly correlation.

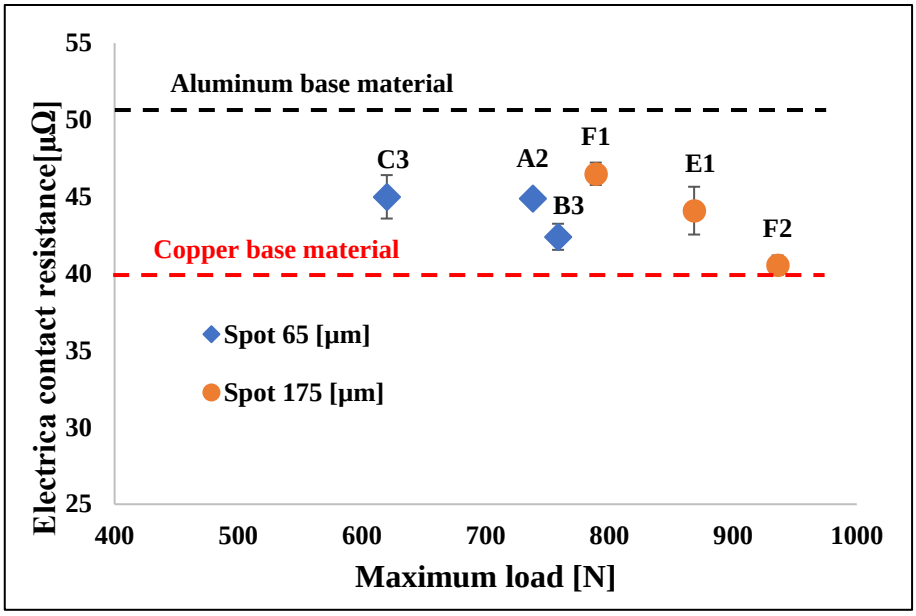

Fig.15 Electrical contact resistance as a function of maximum failure load.

Table 9 summarize the characteristics in terms of weld bead morphology of the samples used for mechanical and electrical tests. From the analysis of the data, it can be seen that there is no linear correlation between the width at the interface and the electrical properties of the joints. The best performances were obtained for weld bead with a particular morphology, in particular when full penetration of the copper in aluminum sheet was avoided; the reason could be that for weld beads with high interface widths and high penetration depths, greater thermal inputs are required with consequent formation of both hard and brittle intermetallic phases which are characterized by greater electrical resistivity.

Table 9: Summary of samples used for electrical and mechanical properties.

Sample	Power [W]	Welding speed [mm/s]	Spot diameter [µm]	Interface width [µm]	Penetration depth [µm]	Maximum load [N]	Electrical contact resistance [µΩ]
C3	1000	250	68	220	390	620	45
A2	600	200		150	230	738	44.9
B3	800	250		220	350	758.5	42.4
F1	1500	150	175	399	400	789	46.5
E1	1250	150		223	60	868	44.1
F2	1500	200		300	150	936	40.5

4. Conclusions

Within this study, thin aluminum (1050) and pure copper sheets were joined by continuous-wave laser welding with different focal lengths in order to study the effects of the focused spot diameter on weld seam properties.

The outcomes of this investigation can be summarized as follows:

- A smaller laser spot allowed welding with lower overall power, thus reducing the total heat input during the process. It also favored a wider process window with better control of penetration depth and mixing of the base materials.
- Due to the physical and optical properties of copper, a larger laser spot required higher power to melt the material. In this case, correct selection of power and speed was difficult because the weld seam transitioned quickly from a no-welding condition to full penetration with the presence of cracks and pores.
- Mechanical properties depended on both energy density and weld bead dimensions, in particular the interface width. The optimum energy density was around 0,5-0,6 MJ/mm^2, achieving tensile loads of roughly 800 N with the larger spot and 700 N with the smaller one. Brittle fracture behavior was recorded with the large spot size, while ductile behavior was recorded with the smaller one.
- Electrical contact resistance was strongly influenced by the weld bead morphology, with best performance achieved where full penetration was avoided. The measured values, obtained with optimized parameters, were about 42 μΩ with smaller spot and 40.5 μΩ with larger one. Highest mechanical strength and lowest contact resistance were achieved with the same process parameters.
- SEM-EDX analysis revealed how a small spot diameter minimized the formation of copper-rich intermetallic compounds, which are detrimental to weld bead properties.

Declarations

Funding: The authors did not receive support from any organization for the submitted work.

Conflicts of interest/Competing interests: The authors declare that they have no known competing financial interests or personal relationships that could have appeared to influence the work reported in this paper.

References

[1] H. Saariluoma, A. Piiroinen, A. Unt, J. Hakanen, T. Rautava, and A. Salminen, “Overview of optical digital measuring challenges and technologies in laser welded components in ev battery module design and manufacturing,” *Batteries*, vol. 6, no. 3, pp. 1–15, 2020. https://doi.org/10.3390/batteries6030047

[2] A. Perner and J. Vetter, *Lithium-ion batteries for hybrid electric vehicles and battery electric vehicles*. Elsevier Ltd., 2015. https://doi.org/10.1016/B978-1-78242-377-5.00008-X

[3] P. A. Schmidt, M. Schweier, and M. F. Zaeh, “Joining of lithium-ion batteries using laser beam welding: Electrical losses of welded aluminum and copper joints,” *ICALEO 2012 - 31st Int. Congr. Appl. Lasers Electro-Optics*, vol. 915, no. 2012, pp. 915–923, 2012. https://doi.org/10.2351/1.5062563

[4] S. Hollatz, P. Heinen, E. Limpert, A. Olowinsky, and A. Gillner, “Overlap joining of aluminium and copper using laser micro welding with spatial power modulation,” *Weld. World*, pp. 513–522, 2020. https://doi.org/10.1007/s40194-020-00848-9

[5] I. Das Chowdhury *et al.*, “Investigation of mechanical properties of dissimilar joint of 6063 aluminium and C26000 copper alloy by friction stir welding,” *Mater. Today Proc.*, vol. 44(6), 4039-4047, 2020. https://doi.org/10.1016/j.matpr.2020.10.219

[6] S. S. Lee *et al.*, “Characterization of ultrasonic metal welding by correlating online sensor signals with weld attributes,” *J. Manuf. Sci. Eng. Trans. ASME*, vol. 136, no. 5, 2014. https://doi.org/10.1115/1.4028059

[7] F. Lerra, A. Ascari, and A. Fortunato, “The influence of laser pulse shape and separation distance on dissimilar welding of Al and Cu films”, Journal of Manufacturing Processes vol. 45, pp. 331–339, 2019. https://doi.org/10.1016/j.jmapro.2019.07.015

[8] F. Fetzer, M. Jarwitz, P. Stritt, R. Weber, and T. Graf, “Fine-tuned remote laser welding of aluminum to copper with local beam oscillation”, *Phys. Procedia*, vol. 83, pp. 455–462, 2016. https://doi.org/10.1016/j.phpro.2016.08.047

[9] T. Solchenbach and P. Plapper, “Mechanical characteristics of laser braze-welded aluminium-copper connections”, *Opt. Laser Technol.*, vol. 54, pp. 249–256, 2013. https://doi.org/10.1016/j.optlastec.2013.06.003

[10] P. Schmalen, P. Plapper, P. Peral, I. Titov, O. Vallcorba, and J. Rius, “Composition and phases in laser welded Al-Cu joints by synchrotron x-ray microdiffraction.”, in *Procedia CIRP*, 2018, pp. 74:27–32. https://doi.org/10.1016/j.procir.2018.08.006

[11] P. Schmalen and P. Plapper, “Evaluation of laser braze-welded dissimilar Al-Cu joints”, *Phys. Procedia*, vol. 83, pp. 506–514, 2016. https://doi.org/10.1016/j.phpro.2016.08.052

[12] A. Ascari, A. Fortunato, E. Liverani, and A. Lutey, “Application of different pulsed laser sources to dissimilar welding of Cu and Al alloys”, *Proc. Lasers Manuf. Conf.*, pp. 1–10, 2019.

[13] V. Dimatteo, A. Ascari, and A. Fortunato, “Continuous laser welding with spatial beam oscillation of dissimilar thin sheet materials (Al-Cu and Cu-Al): Process optimization and characterization,” *Journal of Manufacturing Processes*, vol. 44(2019), pp. 158–165. https://doi.org/10.1016/j.jmapro.2019.06.002

[14] A. Fortunato and A. Ascari, “Laser Welding of Thin Copper and Aluminum Sheets : Feasibility and Challenges in Continuous-Wave Welding of Dissimilar Metals”, pp. 136–157, 2019. https://doi.org/10.1007/s40516-019-00085-z

[15] U. Reisgen, S. Olshock, S. Jakobs and N. Holtum, "Influence of the degree of dilution with laser beam vacumum-welded Cu-Al mixed joints on the electrical properties".Procedia CIRP.Volume 74(2018), pp.23-26.

[16] M. Jarwitz, F.Fetzer, R. Weber and T. Graf, " Weld Seam Geometry and Electrical Resistance of Laser-Welded,

Aluminum-Copper Dissimilar Joints Produced with Spatial Beam Oscillation", Metals, vol. 8(7):510(2018).

[17] S. Yan and Y. Shi, "Influence of laser power on microstructure and mechanical properties of laser welded Al/Cu dissimilar lap joints", Journal of Manufacturing Processes,45(2019), pp.312-321.

[18] D.Zuo et al., "Intermediate layer characterization and fracture behavior of laser-welded copper/aluminum metal joints", Materials and Design, 58(2014), pp- 357-362. https://doi.org/10.1016/j.matdes.2014.02.004

[19] JA. Rayne et al.,"Investigation of interfacial reactions in thin film couples of aluminum and copper by measurement of low temperature contact resistance". Thin Solid Films, 65(1980) , pp.381-391. https://doi.org/10.1016/0040-6090(80)90248-5

[20] H. G. Jiang, J. Dai, H. Tong, B. Ding, Q. H. Song, and Z. Hu, “INTERFACIAL REACTIONS ON ANNEALING CU/AL MULTILAYER THIN-FILMS,” *J. Appl. Phys.*, vol. 74(1992), pp. 6165–6169. https://doi.org/10.1063/1.355183

[21] Y.J. Ko, J, Yoon, J. Lee, J.H. Hann, “Effects of Cu interlayer on the wettability of aluminum on carbon”, Journal of Alloy and Compounds, vol. 574(2013), pp.526-531 http://dx.doi.org/10.1016/j.jallcom.2013.05.190